POAC'23
Glasgow, United Kingdom

Proceedings of the 27th International Conference on
Port and Ocean Engineering under Arctic Conditions
12-16 June 2023, Glasgow, United Kingdom

A Review of Global and Local Ice Pressure Models for Application to FPSO Design for Iceberg-Impacts

Mark K. Fuglem[1], Paul D. Stuckey[1], Hamid Shayanfar[1], Freeman E. Ralph[1], Jan W. Thijssen[1]
[1] C-CORE, St. John's, Canada

ABSTRACT

C-CORE and DNV are conducting a joint industry project to clarify design requirements for iceberg loads on FPSOs operated in offshore regions with icebergs. This requires consideration of impact loads given the FPSO size, shape, directional control and disconnect capability, the mooring system, the iceberg population, environmental driving forces and hydrodynamic interaction effects and the ice detection and management capabilities (Stuckey et al., 2023, Huang et al., 2023). The focus in this paper is on modelling global and local ice strength as required for determining mooring offsets and local structural design. Relevant ice mechanics and ISO 19906:2019 standard is reviewed and pertinent data and models re-examined. It was found that existing models in ISO 19906:2019 are largely sufficient for FPSO design, though nuances on how to apply the models are extremely important, as misuse can result in inaccurate load estimates. This paper aims to show the intended application through example cases.

KEY WORDS: Iceberg; FPSO; Design Loads.

REVIEW OF ICE MECHANICS

The energy imparted to the FPSO during an iceberg impact will depend on the masses of the two bodies, the impact location and angle of the ship plating relative to the impact location, the impact velocities and hydrodynamic effects. Iceberg drift velocities on the Grand Banks average around 0.3 m/s and can exceed 1 m/s in extreme conditions. Wave-induced velocities of bergy bits can exceed 4 m/s in storm conditions. One is then dealing with glacial ice and impacts with strain rates well within the brittle range. Iceberg ice has grains that are granular and randomly oriented with diameters in the order of 5 to 35 mm (Gammon et al., 1983). Internal cracks can form from mechanical stress due to glacier flow and iceberg buoyant forces and from thermal stresses due to temperature differentials (Cammaert and Muggeridge, 1988). Jones (2006) indicates based on small scale tests that the strength of iceberg ice at higher strain rates could be as little as 1/3 that of laboratory ice.

The failure mechanics of ice under higher strain rates is complex. Two important mechanisms have been observed. Near the indentor, damage occurs within a relatively thin layer influenced by the formation of high pressure zones (HPZs), microcracking and microstructural changes to the ice. The majority of the load during an impact is transferred through high pressure zones that cover approximately 10% of the contact area (Figure 1). HPZ pressures exceeding 70 MPa have been observed over very small areas (e.g., 0.0001 m^2); whereas average nominal pressures are in the order of 1 MPa are found on areas about 1 m^2 and larger. HPZs can persist up to several seconds. Away from the indentor the ice remains largely linear elastic and prone to brittle fracture. Spalls may be trigged by the occurrence of HPZ near the periphery of the

contact zone. Large fractures and spalling can influence the geometry of the ice feature and contact area, and change the stress distribution within the ice.

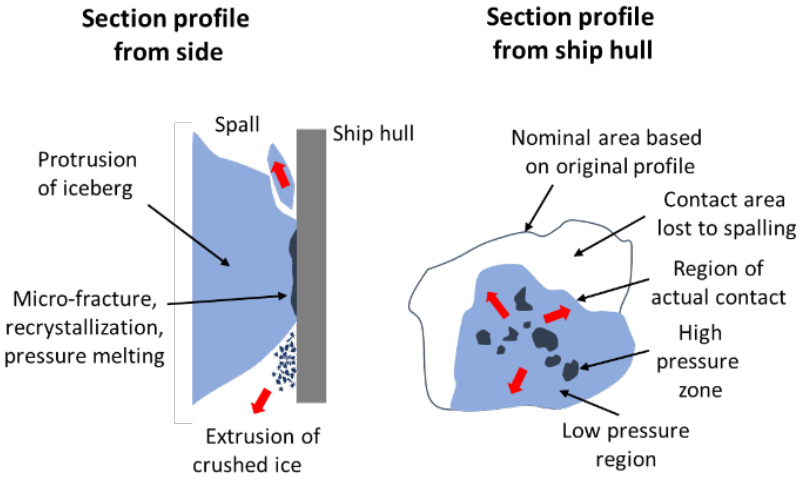

Figure 1. Illustration of ice failure mechanism at fixed point of time during direct impact

The global nominal area is the contact area that would occur with no spalling and no iceberg rotation. This area will increase during a direct impact, as the iceberg slows down (Figure 2). The nominal global pressure is defined as the global force divided by the global nominal area. The global impact force generally increases with contact area; load drops can occur due to spalling events and smaller variations occur as HPZs fail, ice is extruded, and the load builds up again. Nominal global area and pressure are used in empirical load models as it is not practical to estimate actual contact areas, given the randomness of ice fracture process. It has been observed that global pressures decrease in general with area, presumably because the larger areas under high stress are more likely to include larger cracks and defects. Care is required in interpreting pressure-area data where the data represents peak pressures from different events, rather than change in pressure during an event with changing contact area.

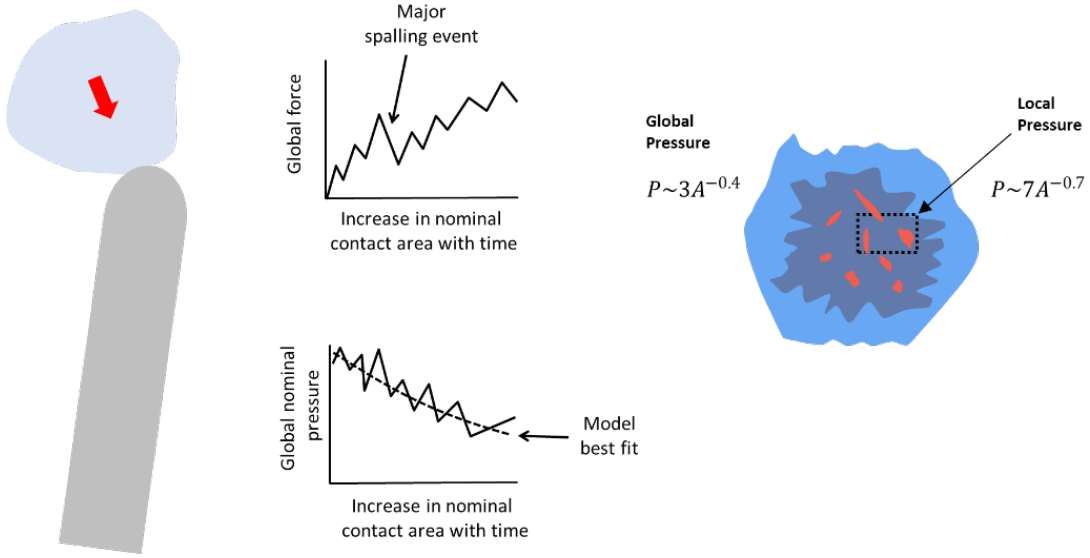

Figure 2. Illustration of forces and pressures during an impact

Understanding how HPZs behave is relevant to better modelling of global and local pressures and spalling events. Figure 3 highlights some of interesting observations. In Medium Scaling Tests at Pond Inlet (iceberg ice) and Hobson's Choice (multi-year ice), different shaped indentors were pushed into ice using hydraulic rams and the forces measured. The top left figure shows the ice face at the end of one of the indentations, as well as an interpretation of where relatively intact (in fact, recrystallized ice) remained (middle figure). For the smaller contact area involved here, the HPZs formed show a pattern, for larger contact areas during ship impacts, the HPZs appear to be randomly situated. The top right figure shows a cross-section taken after a test; there are zones of finely crushed ice, plus a region in the middle with blue 'recrystallized' ice where an HPZ occurred. Jordaan (2001) indicates that micro-fracturing occurs at the outside of an HPZ, and as the pressure builds up at the centre of the HPZ, pressure softening occurs until the HPZ fails, ice is extruded, then the process repeats. The bottom figures show triaxially loaded ice with (left) a low volumetric pressure resulting in micro-fracturing and (right) high volumetric pressure resulting in pressure softening followed by recrystallization. Figure 4 illustrates a damage function for ice developed by Jordaan (2001) that represents these processes given different combinations of deviatoric and volumetric pressure. Turner (2018) models HPZs using FEA with more detailed damage functions to study the possible influence of ice temperature and strain rate.

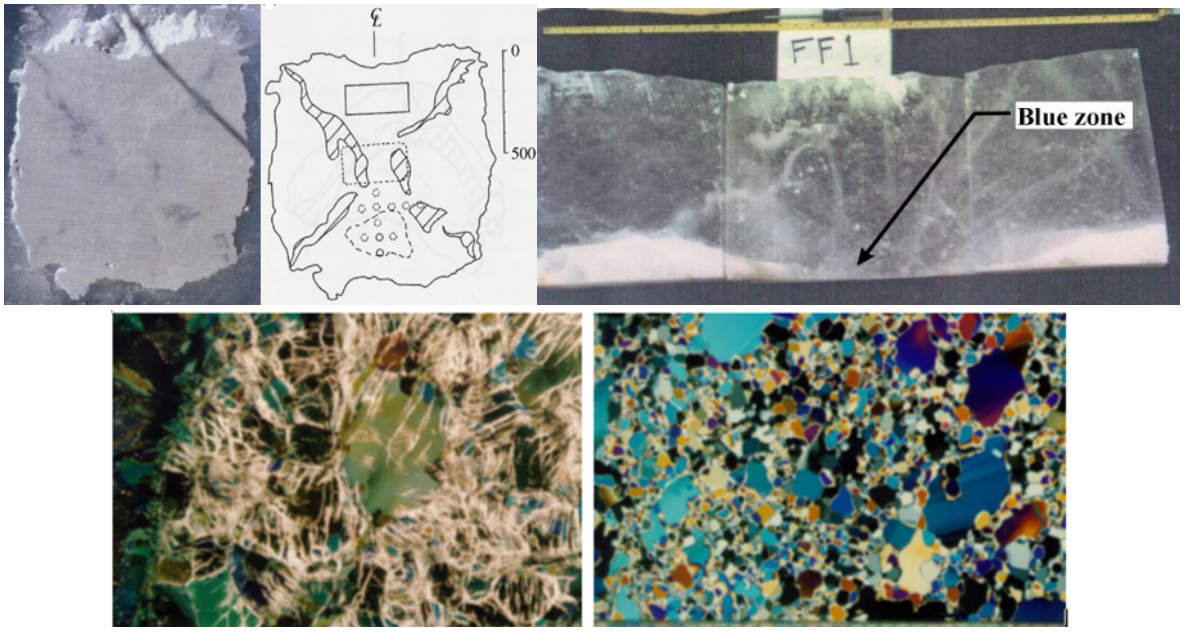

Figure 3. Top left and middle: photograph and interpretation of pattern of ice failure from Medium Scale Tests (Riska, 2018, based on Muhonen, 1991); top right: thin section including damaged layer adject to contact face (along bottom), from Hobson's Choice (Jordaan, 2001); bottom left and right: thin sections of ice for low and high confinement cases respectively from laboratory tests (Meglis et al., 1999)

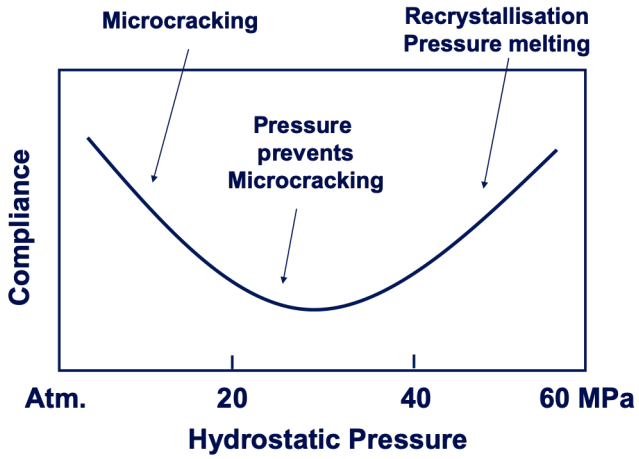

Figure 4. Schematic of compliance as a function of volumetric (hydrostatic) pressure (based on Jordaan, 2001)

While significant improvements in understanding and modelling HPZs have been achieved, it is still not practical to model ice failure loads using constitutive models. It is also not feasible to scale up lab test data given large scale effects and the sensitivity of ice loads to specific conditions. Ice failure processes are also very random; this is critical to take into account when selecting design loads. Ice strength calculations for structural design are generally based on empirical models calibrated to large scale test data. As limited information is available on the full-scale strength of glacial ice, data for interactions with multi-year ridges (primarily ship ramming loads) are typically included; multi-year ice is largely brine free and has similar properties as glacial ice.

ISO 19906:2019 GLOBAL LOAD MODEL

ISO 19906:2019 Section A.8.2.4.3.5 'Global ice pressures from ship ramming tests' provides a probabilistic method that has been used for simulating loads during an iceberg impact. The model is of the form

$$P_G = C_p A_N{}^{D_p} \quad (1)$$

where A_N is nominal global contact area, and C_p and D_p are random coefficients calibrated based on the analysis of a large database of ship rams with multi-year ice. ISO 19906:2019 suggests a lognormal distribution for C_p with a mean of 3.0 MPa and a standard deviation of 1.5 MPa and a normal distribution for D_p with a mean of –0.4 and standard deviation of 0.2. While the model is generally reasonable over the range of nominal contact areas for which it was calibrated (typically up to 10 m^2 and in cases up to 30 m^2 or more), the predicted loads for areas larger than 30 m^2 has been critically reviewed. It is stated in ISO 19906:2019 that a lower bound cut-off for the pressure-area curve should be considered for large contact areas.

ISO 19906:2019 LOCAL AND BACKGROUND LOADS

ISO 19906:2019 Section A.8.2.5.3 'Probabilistic model for local ice pressures' provides a method for determining design local ice pressure, p, as a function of annual probability of exceedance, $1 - F_P$, local structural area, A, and exposure, μ, expressed in terms of iceberg impact rate and average impact duration:

$$p = x_0 + \alpha\{-\ln[-\ln F_P] + \ln \mu\} \quad (2)$$

where $\alpha = B_P A^{-0.7}$ is a parameter (in MPa) that depends on local area and the nature of the ice interaction, B_P, is an empirical coefficient, x_0 is a constant representing the position of the design distribution (in MPa) and $\mu = \nu r t/0.7$, where ν is the expected annual number of events, r is the probability that an events hits the local area of interest and t is the expected impact duration. Figure 5 shows different curves for α, determined based on different ship trials, where C in the table is the same as B_P. The curves with higher values of B_P generally correspond to voyages in more severe ice conditions. The curve with the highest B_P is based on an analysis of Kigoriak rams with heavy multi-year ridges.

ISO 19906:2019 Section A.8.2.5.5 "Local Ice Pressure Combinations" indicates that when checking local structural capacity with respect to local pressure, it may be appropriate to consider the influence of background pressure over an appropriate area around the local area. The background area and pressure could correspond to the global load or to an area defined by larger framing. While some references are provided for determining global nominal pressure, no guidance is provided for determining background pressures over specified structural areas containing the local area of interest.

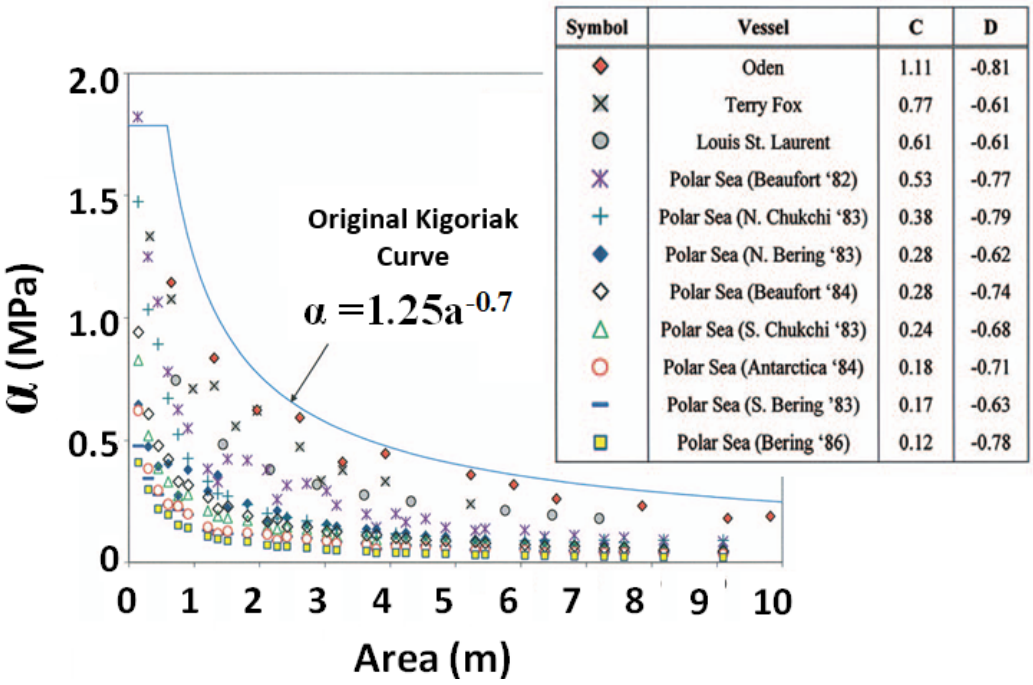

Symbol	Vessel	C	D
◆	Oden	1.11	-0.81
×	Terry Fox	0.77	-0.61
○	Louis St. Laurent	0.61	-0.61
✳	Polar Sea (Beaufort '82)	0.53	-0.77
+	Polar Sea (N. Chukchi '83)	0.38	-0.79
◆	Polar Sea (N. Bering '83)	0.28	-0.62
◇	Polar Sea (Beaufort '84)	0.28	-0.74
△	Polar Sea (S. Chukchi '83)	0.24	-0.68
○	Polar Sea (Antarctica '84)	0.18	-0.71
–	Polar Sea (S. Bering '83)	0.17	-0.63
□	Polar Sea (Bering '86)	0.12	-0.78

Figure 5. Local pressure parameter α vs. local contact area for Oden, Terry Fox and Polar Sea trials; (Jordaan et al. 2007; Taylor et al. 2010)

REEXAMINATION OF DATA AND MODELS

HPZ Modelling of Ice Pressures

HPZ modelling can provide insight into the distribution of ice pressure where data is limited and as such, the method is explored in further detail here. Ralph and Jordaan (2017) provide background on the modelling of ice pressures based on random simulation of HPZs. The method was used previously for modelling line loads on ships travelling through level ice by a number of authors. High local loads are assumed to occur at random locations with the number of loads Poisson distributed and the forces exponentially distributed. The total force then

follows a compound Poisson process. HPZs characteristics (density and force distributions) have also been estimated for ice breaker (CCGS Louis S. St. Laurent and Kigoriak) impacts with multi-year floes and ridges using pressure sensor and strain gauge measurements and then used to simulate ice pressures (Johnston, 1993, Johnston et al., 1998, Zou, 1996). The Polar Sea icebreaker conducted a number of trials in the 1980's, using a 9.1 m^2 strain gauge panel with 60 subpanels of size 0.15 m^2 to measure local pressures. Ralph and Jordaan (2017) provide estimates of HPZ characteristics based on this data and using Monte-Carlo methods simulated local pressures resulting in alpha curves very similar to those in ISO 19906:2019. During interactions, one expects HPZs to form, last a very short period of time then disappear. One could model the life spans of HPZs explicitly, estimating how they grow and decay. Ralph (2016), showed that in the case of the Polar Sea, pressures could be matched by modelling independent sets of HPZs approximately every three seconds during interactions; one would expect this value as determined through calibration to relate to a characteristic autocorrelation statistic**.** The Compound Poisson-Exponential distribution can be modeled in closed form in terms of a Bessel function of the first kind, but we have found it to be more practical and general to implement a Compound Poisson-Gamma distribution in terms of weighted sums of Gamma distributions, using the fact pointed out by Jordaan (1993b) that the sum of n Gamma distributed forces results in a Gamma force distribution with a mean n times greater and standard deviation reduced by a factor $1/\sqrt{n}$. Subroutines have been implemented for the corresponding probability density function, cumulative distribution function and for generating random numbers. Special care is required for the discrete probability of a zero load.

A number of questions arise when applying HPZ models. In the modelling work described above, the HPZs are assumed to be independent and identically distributed (IID), evenly distributed over the contact region, and consistent over the duration of the interaction. The HPZ model can then be defined simply in terms of HPZ density ρ, mean HPZ force μ and characteristic duration τ. These parameters have been found to vary for different ship trials. Questions of interest are how these parameters vary with ice temperature, strain rates and confinement and how well the assumptions regarding independence and stationarity hold.

Polar Sea 1982 Trials

A decision was made to further investigate local pressure data from the 1982 trials, given the relatively high resolution of the data and the high percentage of multi-year ice encountered. The trials took place from September 28 through October 16, just to the east of Point Barrow (St. John et al., 1984). A review of the temperatures data (NOAA, 2021) shows that the air temperature at Point Barrow was around -5°C until October 5th, dropped to -15°C by October 8th, then -20°C by October 16th. We did not find information on ice temperatures but a comparison can be made to information for similar trials in the same region from September 29 to October 13, 1985. Here the temperature remained around -5°C, with two days above 0°C around October 7th and a four-day cold period (about -10°C) around October 10th. Cores taken during the 1985 period show that while ice temperatures at the surface reflect the air temperature, the ice temperature at 1 m depth was typically between -2 and -4°C. One might expect a similar finding in 1982, though the air temperatures were somewhat colder. Figure 6 shows the maximum average pressures over 9.1 m^2 as a function of date for 1982 trials, there may be some correlation to air temperature, but the data is limited. Figure 7 shows maximum average pressure over 0.15 m^2 (left) and force over 9.1 m^2 (right) for impacts with multi-year ice during the 1983 North Chukchi Sea Trials (St. John et al., 1984). For velocities greater than 2 m/s, there is no discernible trend.

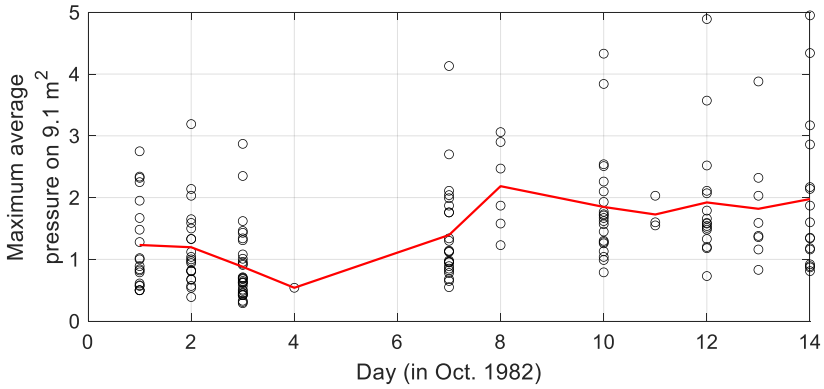

Figure 6. Maximum average pressures over 9.1 m^2 as a function of date for 1982 trials

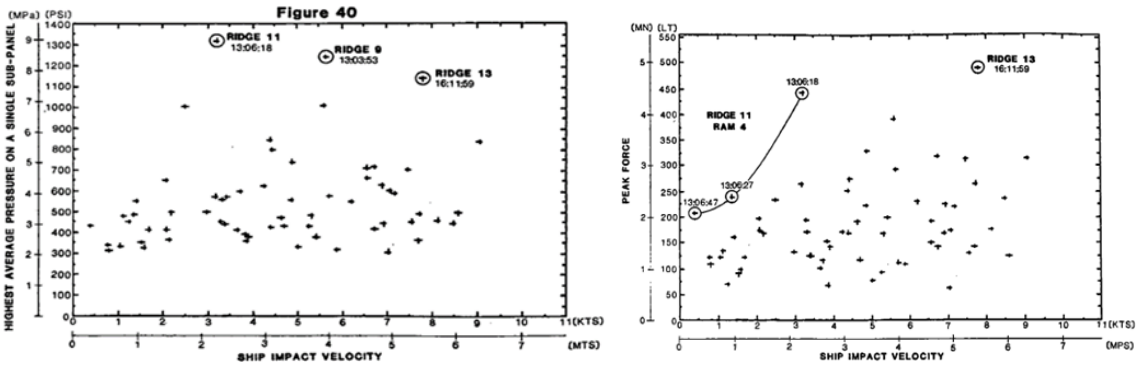

Figure 7. Maximum average pressure over 0.15 m^2 (left) and force over 9.1 m^2 (right) 1983 North Chukchi Sea Trials (St. John et al., 1984)

Local pressure events involving impacts with multi-year ice were selected from the 1982 trials. All events were included except those that consisted of the vessel pushing floes. Some judgement was required, given that the descriptions of the impacts were limited. The data includes impacts with floes, ramming of ridges and clipping floes. The highest recorded pressures on single 0.15 m^2 subpanels appears to be from impacts with floes, having short duration and limited total area of contact. Other events were of longer duration and one can see how HPZs (as observed through loads on the 0.15 m^2 subpanels) moved across the 9.1 m^2 panel (Figure 8).

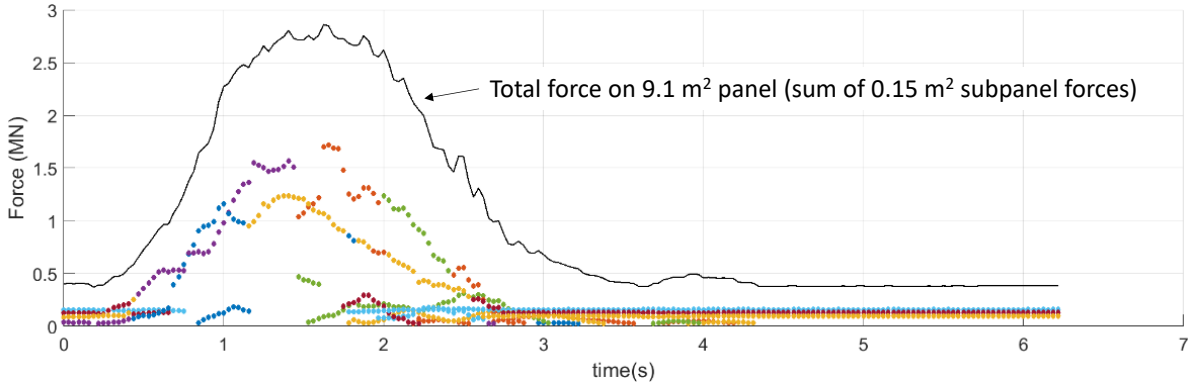

Figure 8. Example time trace of force on 9.1 m^2 panel and individual 0.15 m^2 subpanels

A check was made to determine the uniformity of loadings on the different subpanels (Figure 9). The numbers represent the fraction of the 98 selected events for which a threshold value was exceeded at the time during the interaction when the maximum single subpanel load

occurred. It is of note that the counts are quite non-uniform; this may reflect differences in the strain gauge sensitivity and how the panel was calibrated for loads. Note that the bottom three rows were loaded more often than the top three rows; this could relate to the vertical location of the panel relative to the water line and where ice features were first impacted.

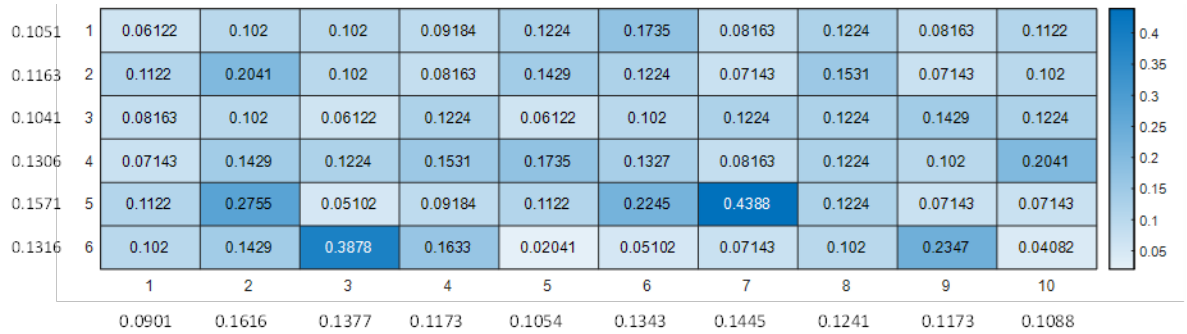

Figure 9. Proportion of time subpanel loads exceeded threshold (mean values shown outside)

A check was then made on the independence of loads on the different subpanels. Figure 10 shows the conditional probability of the different subpanels having loads that exceed the threshold, conditional on a specific subpanel, in this case Row 5 Column 7 (R5C7), being loaded. The counts were weighted by the inverse of the counts in Figure 9 to remove the effect of the non-uniformity of readings. It is of interest that when subpanel R5C7 is loaded, there is a more distinct loading of the bottom rows relative to the top rows. The reverse was found when dependencies on loading of subpanels in the top row were considered. Figure 11 summarizes the dependency as a function of distance to the reference subpanel. There appears to be a small dependency based on the mean trend line, with the correlation dropping off with distance; this could relate to the preferential loading on the bottom or top of the panel in different interactions. Note that one expects some correlation for the neighbouring subpanels as HPZs may occur on the border of the reference and neighbouring subpanels.

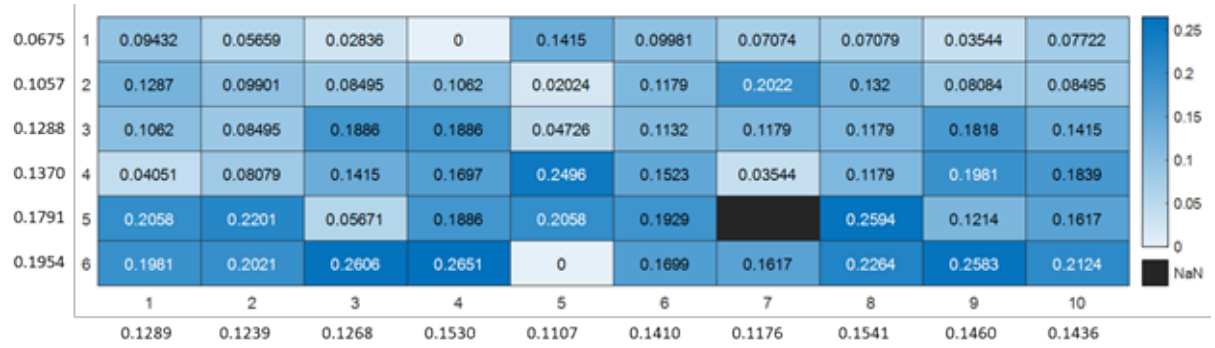

Figure 10. Conditional probability of subpanel loads exceeding threshold, given subpanel R5C7 is loaded.

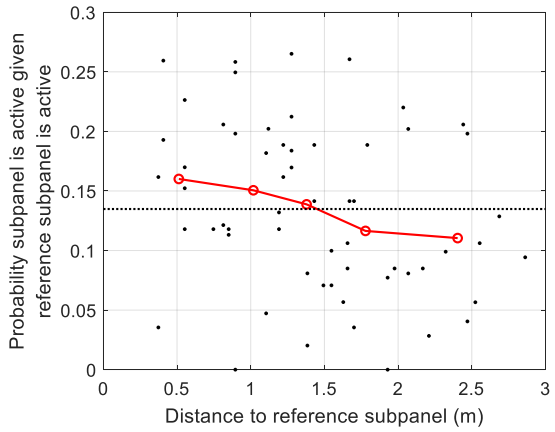

Figure 11. Probability subpanel is active, conditional on reference subpanel R5C7 being active, as a function of distance to reference subpanel

A direct check was made regarding the dependence between local and background pressure. Three different combinations of local and background area were analyzed, and similar findings were found for all. Figure 12 shows the results for one example. The local pressure is the maximum value for the event and the background pressure is the value at that same time. The top left figure shows background (P_B) versus local (P_L) pressure; there appears to be a definite correlation. The top right figure shows how the average subpanel load changes, whereas the bottom left figure shows how the number of active subpanels changes. This shows that as the local pressure increases, in the background area both the number of active subpanels and the mean force on the subpanels increases. The dependency here relates more to differences in loadings on subpanels in different interactions, whereas the analysis on dependence relates to the dependency of loadings within given interactions.

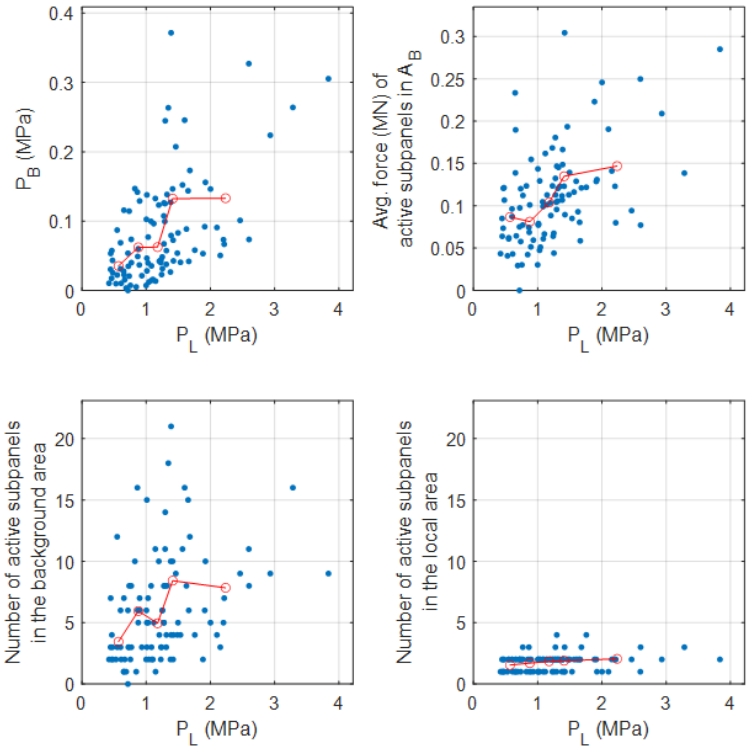

Figure 12. Local and background pressure combinations; A_L = 0.6 m^2; A_B = 8.5 m^2 (i.e. 9.1-0.6 m^2)

Terry Fox Bergy Bit Impact Trials

The Terry Fox Bergy Bit Impact Study was carried out from June 18th through 23rd, 2001 off northern Newfoundland. Information on the study can be found in Ritch et al. (2008). The study is important as a key data source for local pressure measurements involving ship impacts with icebergs. The Terry Fox is an 82 m long icebreaker with a displacement of 6,700 t. Several systems for measuring loads were used; the study here is based on the 5.23 m^2 strain gauge panel used. Ritch et al. (2008) determined maximum average pressures corresponding to local areas from 0.33 to 5.23 m^2; Figure 13 shows load exceedance plots given iceberg mass.

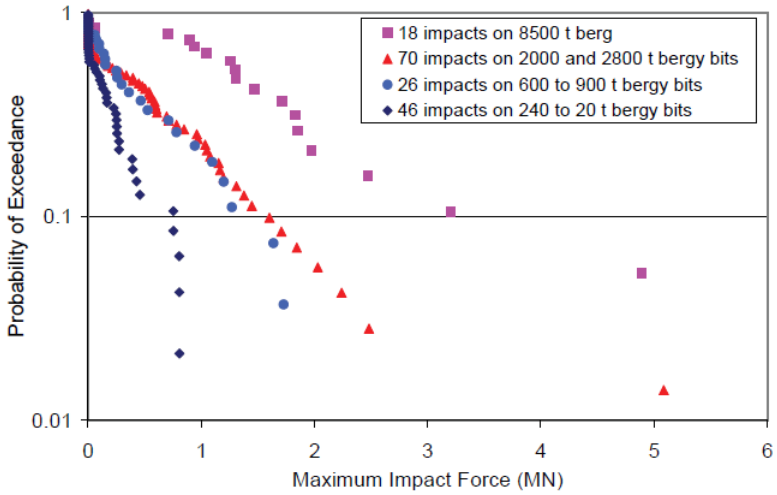

Figure 13. Load exceedance plots as a function of iceberg mass (Ritch et al., 2008)

An approximate analysis was conducted to determine if the differences could be explained in terms of exposure (amount of ice crushing). Impacts were simulated for a similar range of iceberg mass and vessel velocity. For each impact the amount of ice crushed was related to the iceberg mass and vessel velocity squared. The code referenced earlier to simulate random local pressure values for a compound Poisson distribution was applied. Input parameters were adjusted to achieve a rough fit for the 8,500 t case (Figure 14). It was not possible to get different slopes on the curves using the same HPZ parameters; this would require using different values of HPZ average force depending on mass. Ralph (2016) also points out that the slope depends on the HPZ average force, not density. It appears that either the local pressures are influenced by ice temperature (i.e. colder ice reached in more severe impacts) or confinement (larger contact areas for more severe impacts).

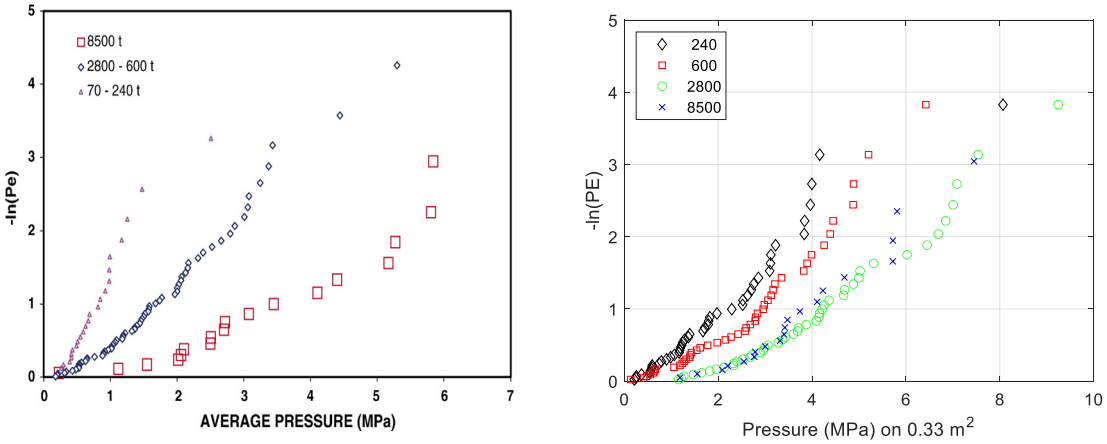

Figure 14. Left: load exceedance plot as a function of iceberg mass (Ritch et al., 2008); right: approximate simulation based on exposure only

Selection of Background Pressure

ISO 19906:2019 does not provide clear guidance on selecting background pressures associated with extreme-level (10^{-2}) and abnormal-level (10^{-4}) local pressures, except when the background pressure is determined from the global load. If one can show that the structure is safe for an envelop of local and background pressures (Figure 15, left) such that the annual probability of an impact resulting in a local and background pressure combination to the right of the curve is less than the specified APE, this is sufficient. Note that generally, the maximum local pressure is greater than the maximum background pressure, else the local area considered would be moved. One would need to determine the joint probability distribution for P_L and P_B and ideally pick a curve that does not result in excessive over design.

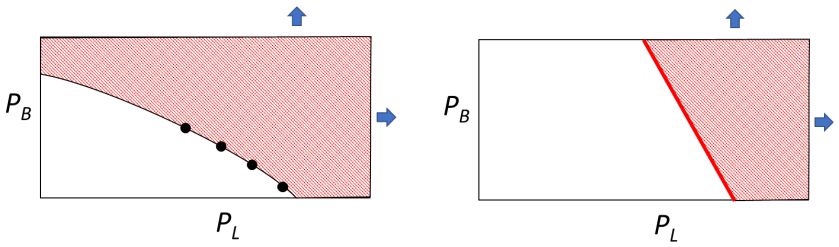

Figure 15. Strategies for determining local and background pressure combinations

An approximate solution is considered here in which the equation in ISO 19906:2019 used to determine the local pressure on A_L is also used to determine the pressure over the area A_L+A_B, both for the same APE. Figure 16 shows an example of background pressures that result. Consider the local pressure P_L* and background pressure P_B* determined this way for annual probability of exceedance (APE) of 10^{-4}. Preliminary analyses of background effects on strains shows that the background pressure results in a 10 to 20% increase in strain for the particular structure considered. As an example, consider that the failure curve is of the form $P_L + P_B/5$ equals a constant, and goes through (P_L*, P_B*) as shown by the red line in Figure 17 (left side). If P_L and P_B are perfectly correlated, then the annual probability of being in the red zone is also 10^{-4}. If P_L and P_B are independent, the probability of being in the blue zone is $1 - 2 \cdot 10^{-4}$ so the probability of being outside this zone is $2 \cdot 10^{-4}$ (i.e., two times the target APE). The probability of being to the right of the red line will be less than this. An example check is made here to explore if this is conservative and potentially by how much, assuming IID HPZs. Random sets of HPZ's were modelled for a 1 m^2 local area and a 5 m^2 background area (Figure 17, right).

Based on the simulated points, the local pressure P_L* and background pressure P_B* associated with APE 10^{-4} were determined. The probability of being to the right of the red line in this case was then found to be $7.8 \cdot 10^{-5}$. This test suggests that using (P_L*, P_B*) as defined may provide a slightly conservative method for selecting a background pressure.

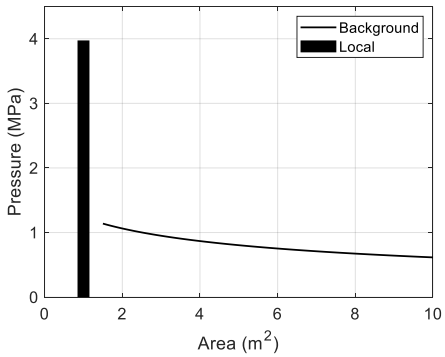

Figure 16. Local pressure on 1 m^2 and background pressure on different areas based on Terry Fox α-curve in ISO 19906:2019 and APE = 10^{-4}.

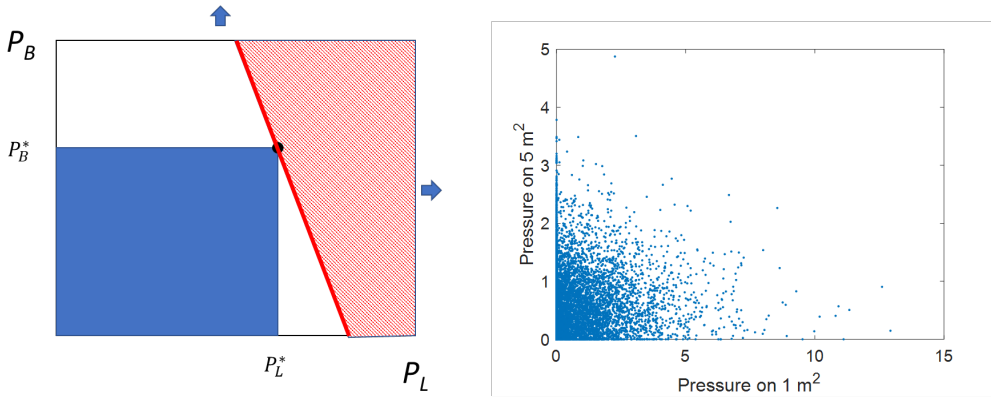

Figure 17. Illustration showing effect of how picking APE 10^{-4} independent values of P_L and P_B for design would influence probability of exceeding given failure curve (left); random simulation of P_L and P_B (right).

Alternative Global Load Model

The global pressure model referenced in ISO 19906:2019 consists of a power law, with random coefficients, giving pressure as a function of contact area. The exponent is normally distributed with a mean of -0.4 (such that the pressure generally decreases with increasing contact area) and a standard deviation of 0.2. The coefficients were calibrated based on ship ramming data, with consideration of previous work on scaling of ice loads (Carter et al., 1995). C-CORE typically puts limits of -1 to 0.1 on the exponent and an upper limit of 6 MPa on the constant when modelling iceberg loads; in addition, the pressure is not decreased further once a contact area of 50 m^2 is reached.

It has been recognized that the random coefficients allow too much variance in loads, which becomes important for loads at higher exposures. For example, direct application of the model to regions such as Greenland, where icebergs are much more frequent, results in unrealistic pressures. The application of a model based on simulation of HPZs has potential for significant improvement; some preliminary work is presented here. Figure 18 shows a global pressure-area curve that results when the global area is populated with independent and identically

distributed (IID) HPZs. The variance in the pressure decreases with increasing area, as a result of probabilistic averaging. The pressure tends to a constant value equal to the HPZ density times mean pressure. Figure 19 shows comparisons of the ISO 19906:2019 global pressure model (left) and an HPZ (right) model results versus observed maximum vertical loads from the Kigoriak 1983 Spring ramming trials. It is seen that the HPZ model can provide similar goodness of fit levels. More importantly, the HPZ model is not subject to issues associated with large areas and large numbers of impacts.

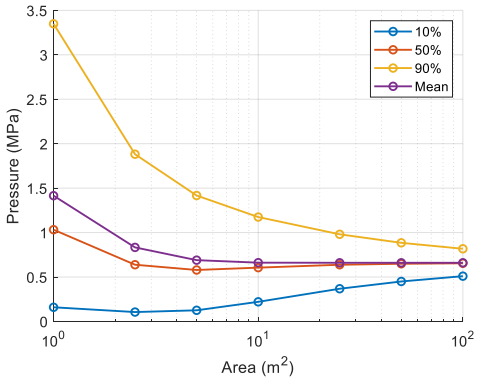

Figure 18. Example global pressure area curve based on HPZ model

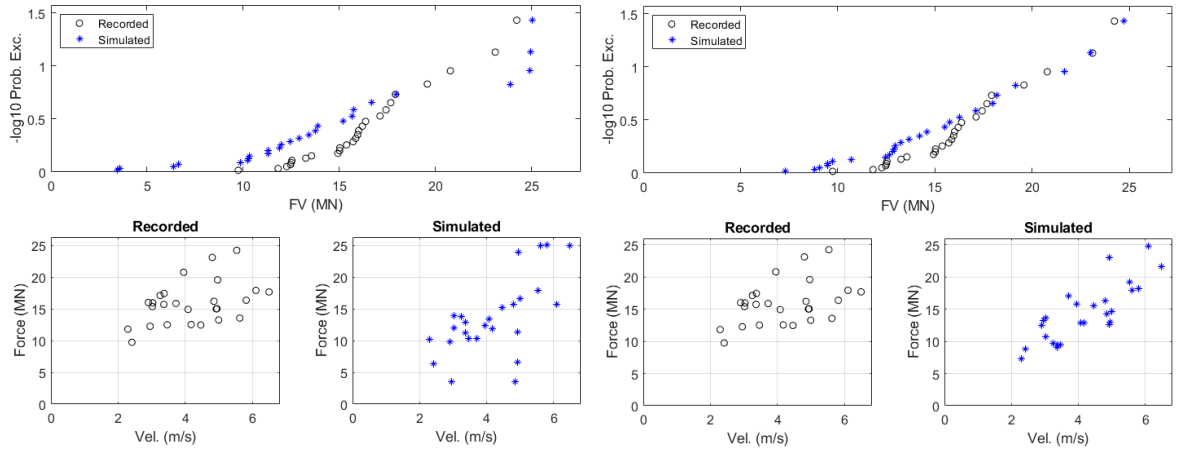

Figure 19. Example comparison of global load distributions based on ISO 19906:2019 model (left) and HPZ (model) right

CONCLUSIONS

Ice failure loads are very random, scale dependent and difficult to model analytically. This necessitates use of empirical models based on full scale that account for the randomness of the loads and exposure in terms of frequency of impacts and durations. Data shows that impact velocity (and hence strain rate) has minimal influence for interactions at speeds greater than 2 m/s. Given the uncertainty in the influence of parameters such as temperature and confinement, it is important to make sure that models used for a given application have been calibrated based on similar ice conditions, interaction parameters, and failure modes. Iceberg loads are generally very rare, making consideration of exposure that much more important.

This work explains some of the issues related to local and global pressures in terms of random behaviour of HPZs, calibrated based on full-scale data. In this initial work, the HPZs have been treated as IID and randomly located over the contact area. While this model explains much of

the observed variance in loads, and exposure clearly plays a very critical role, it does not on its own completely explain all aspects of observed of full-scale test data.

The models presently referenced in ISO 19906:2019 are based on the best full-scale data available, and involve contact areas and interaction velocities generally in line with those expected during iceberg impacts. The ice temperatures for the multi-year features may have been on the warm side in many of the trials, relative to iceberg ice, and there is a lack of specific data on the specifics of many of the interactions. The study by Frederking and Ritch (2009) gives some indication that local pressures increase with impact severity in addition to exposure, whether primarily a result of confinement effects or colder ice temperatures at greater penetrations is uncertain. HPZ type models show promise to address some of these issues if the effects of temperature and confinement can be better defined. It may also be necessary to account for some level of dependence between density and force magnitudes of HPZs. The use of HPZ modelling for assessing global loads shows promise to address some of the concerns with the present ISO 19906:2019 global pressure model.

Further investigation in the following areas would be useful: better definition of the influence of confinement and ice temperature on the density and strengths of HPZs; further investigate dependencies between numbers and load magnitudes of HPZs; and better define the durations of HPZs and factors influencing how long they last. Additional field data, focused on answering the above questions, would also be very valuable.

ACKNOWLEDGEMENTS

The authors would like to acknowledge funding from the JIP participants: Equinor, Aker Solutions, Cenovus, Kvaerner Canada, Oil and Gas Corporation of Newfoundland and Labrador (OilCo), Suncor and TechnipFMC; from the Atlantic Canada Opportunities Agency (ACOA) and from the Newfoundland and Labrador Department of Industry, Energy and Technology. They would also like to acknowledge significant initial input from Dr. Ian Jordaan.

REFERENCES

Cammaert, G., Muggeridge, D., 1988, *Ice interaction with offshore structures*. New York, USA: Van Nostrand Reinhold.

Carter, J., Daley, C., Fuglem, M., Jordaan, I., Keinonen, A., Revill, C., Butler, T., Muggeridge, M., and Zou, B., 1995, *Maximum Bow Force for Arctic Shipping Pollution Prevention Regulations - Phase II*. Memorial University of Newfoundland, Ocean Engineering Research Centre. Submitted for Canadian Coast Guard Arctic Ship Safety.

Frederking, R. and Ritch, R., 2009. *The Nature of the Process Pressure-Area Relation from CCGS Terry Fox Bergy Bit Impacts*, ISOPE

Fuglem, M., Jordaan, I., 1999. *Estimation of Maximum Bow Force for Arctic Vessels*, Ice in Surface Waters

Gammon, P., Gagnon, R., Bobby, W., Russell, W., 1983, *Physical and Mechanical Properties of Icebergs*, OTC-4459-ms.

Huang, Y., Shipilova, O., Mattson, F., and Stuckey, P., 2023, *Influence of Hydrodynamic Effects on Ice Design Loads for FPSOs in Regions with Icebergs*. In Proceedings of 27th International Conference on Port and Ocean Engineering under Arctic Conditions. Glasgow, United Kingdom, 2023.

ISO 19906 (2019), *Petroleum and Natural Gas Industries—Arctic Offshore Structures*, International Organization for Standardization, Geneva, Switzerland.

Jones, S., 2006, *Comparison of the Strength of Iceberg and Other Freshwater Ice and the Effect of Temperature*, PERD/CHC Report 20-83.

Johnson, M., 1993. *Variation of Local Pressures during Ice–Structure Interaction*, M. Eng. Thesis, Faculty of Engineering and Applied Science, Memorial University of Newfoundland.

Johnston, M.E., Croasdale, K.R. and Jordaan, I.J., 1998. *Localized pressures during ice–structure interaction: relevance to design criteria*. Cold Regions Science and Technology 27, 105–117

Jordaan, I. J., 2001, *Mechanics of Ice-Structure Interaction*, Eng. Fract. Mech., 68(17–18), pp. 1923–1960.

Jordaan, I., Xiao, J., Zou, B., 1993, *Fracture and Damage of Ice Towards Practical Implementation*, ASME.

Jordaan, I. J., Li, C., Mackey, T., Stuckey, P., Sudom, D., and Taylor, R., 2007. *Ice Data Analysis and Mechanics for Design Load Estimation*, Final Report, prepared for NSERC, C-CORE, Chevron Canada Resources, National Research Council of Canada, Petro-Canada and Husky Energy.

Jordaan, I.J., Maes, M.A., Brown, P.W., and Hermans, I.P., 1993a. *Probabilistic analysis of local ice pressures*. Proceedings, 11th International Conference on Offshore Mechanics and Arctic Engineering, Calgary, AB, Vol. II, pp. 7-13.

Jordaan, I., Xiao, J, Zou, B., 1993, *Fracture and Damage of Ice Towards Practical Implementation*, ASME

Meglis, I., Melansson, P., Jordaan, I., 1999, *Microstructural change in ice - II. Creep behavior under triaxial stress conditions*, J. Glaciology

Muhonen A., 1991. *Medium scale indentation tests—PVDF pressure measurements, ice face measurements and interpretation of crushing video*. Client Report to National Research Council of Canada, Canadian Hydraulics Center by Helsinki University of Technology, Ship Laboratory, 20 February 1991.

NOAA, 2021, National Centers for Environmental Information. *Downloaded Point Barrow temperature data*. https://www.ncei.noaa.gov/access/search/data-search/global-hourly

Ralph, F., 2016, *Design of Ships and Offshore Structures: A Probabilistic Approach for Multi-Year Ice and Iceberg Impact Loads for Decision-making with Uncertainty*, Memorial University of Newfoundland, PhD Thesis

Riska, K., 2018., *Ice edge failure process and modelling ice pressure*, Phil. Trans. R. Soc.

Ritch, R., Frederking, R., Johnston, M., Browne, R., and Ralph, F., 2008, *Local Ice Pressures Measured on a Strain Gauge Panel during the CCGS Terry Fox Bergy Bit Impact Study*. Cold Regions Science and Technology, Bergy Bits., 52, no. 1: 29–49.

St. John, J., Daley, C., and Blount, H., 1984, *Ice Loads and Ship Response to Ice: USCG Polar Class 1982/1983 Deployment* Prepared for Transport Canada. Report No. TP 6039E.

Stuckey, P., Birknes-Berg, J., Christian, O.E., and Fuglem, M., 2023, *Glacial Ice Impact Loads on Floating Production Facilities*. In Proceedings of 27th International Conference on Port and Ocean Engineering under Arctic Conditions. Glasgow, United Kingdom, 2023.

Taylor, R., Jordaan, I., Li, C., and Sudom, D., 2010. *Local Design Pressures for Structures in Ice: Analysis of Full-Scale Data*. Journal of Offshore Mechanics and Arctic Engineering, 132(3).

Turner, J., 2018, *Constitutive behaviour of ice under compressive states of stress and its application to ice-structure interactions*, PhD Thesis, Memorial University of Newfoundland, St. John's, Canada.

Zou, B., 1996. *Ships in Ice: The Interaction Process and Principles of Design*, PhD Thesis, Memorial University of Newfoundland, St. John's, Canada.